Heritage Science

RESEARCH

Open Access

The biological contribution to the weathering of limestone monuments in a vegetated urban area: results of a 5-year exposure

Paloma Reboah[1,2*], Aurélie Verney-Carron[1], Samir Abbad Andaloussi[2], Vanessa Alphonse[2], Olivier Lauret[1], Sophie Nowak[3], Anne Chabas[1], Mandana Saheb[1] and Clarisse Balland-Bolou-Bi[2]

Abstract

Biological activity, climate and pollution are responsible for the degradation of building stones, especially limestone, which is widely used in the Paris region. In order to determine the respective contribution of physicochemical and biological processes to the degradation of limestone, limestone specimens from the Père-Lachaise cemetery (Paris, France) were exposed for five years under different conditions: sheltered from or exposed to rain and in horizontal or vertical position. After exposure, the collected samples were characterized by light and electron microscopy, X-Ray diffraction and ion chromatography after elution. The results showed an intense biocolonization of the samples exposed to rain, while the sheltered samples were more affected by the pollution (soiling). The characterization of the bacterial and fungal communities using Next Generation Sequencing Illumina 16S for bacteria and ITS for fungi highlighted that five main bacterial phyla were identified: Actinobacteriota, Bacteroidota, Cyanobacteria, Proteobacteria and Deinococcota (major genera *Flavobacterium*, *Methylobacterium-Methylobacter*, *Sphingomonas*, *Roseomonas* and *Nocardiodes*). Among the fungi, the phylum Ascomycota was predominant with the genera *Cladosporium*, *Ramularia*, *Aureobasidium* and *Lecania*. However, the alteration of the limestone is difficult to quantify at this stage. Potassium nitrate of rain origin has been found in the sheltered area, but no gypsum. Therefore, the biocolonization is a fast phenomenon on the stone and the physico-chemical processes derived from it, caused by climate and pollution, are slower. This is in agreement with the long-term observations made on old and unrestored graves of the cemetery described in the literature.

Keywords Bio-deterioration, Limestone, Microbial communities, Preservation, Biological colonization, Exposure campaign

Introduction

Lutetian limestone (43 million years) is widely used in buildings in the northern part of France due to its proximity, with a lot of quarries located in and around the Paris region [1]. Over time, the monuments made out of limestone are exposed to various physical, chemical and biological processes, which can induce their deterioration. The intensity of degradation depends on intrinsic and extrinsic factors. Intrinsic parameters are related to the characteristics of the stone: chemical and

*Correspondence:
Paloma Reboah
preboah@lisa.ipsl.fr
[1] Laboratoire Interuniversitaire des Systèmes Atmosphériques (LISA), Univ. Paris Est Creteil and Université Paris Cité, CNRS, 94010 Créteil, France
[2] Laboratoire eau, Environnement et Systèmes Urbains (LEESU), Univ. Paris-Est Creteil, Val de Marne, Ecole des Ponts, 94010 Créteil, France
[3] Université Paris Cité, CNRS, ITODYS (UMR, 7086), 75013 Paris, France

mineralogical composition, porosity, and roughness. Extrinsic parameters include climate, pollution, and biological organisms.

First, climate plays an important role on the natural limestone degradation and particularly meteorological parameters (rain, wind, insolation, relative humidity, temperature) that can induce physico-chemical deterioration, such as erosion, loss of material, salt crystallization (by alternation of moisture – drying) [2], change of the porosity (by freeze–thaw cycles in presence of water on porous network) [3], etc.

Then, the natural alteration is generally increased by the atmospheric pollution (gaseous pollutants and particular matter). Air pollution interacts with limestone through dry (in absence of rain) or wet deposition (in presence of rain). Black crusts are an example of dry deposition. They correspond to the crystallization of gypsum ($CaSO_4{\cdot}2H_2O$) by reaction between Ca from the stone and atmospheric SO_2. On a monument, they are preferentially found in sheltered part from rain [4, 5]. Wet deposition is affected by acidification of the rain, that takes place directly in the cloud or during rainfall by washing of atmospheric pollutants suspended in the lower atmosphere [6].

Stones can also be colonized by microorganisms such as fungi, bacteria, cyanobacteria, mosses, lichens, or algae [7–10].

Over a period of 5 years to several decades, it can be expected that biocolonization will cause biodeterioration in addition to the aesthetic impact. The growth of mosses can cause serious damage to stone monuments and appears to occur later than the other organisms. They are attached to the substrate by small structures called rhizoids, which expand and contract to break down the stone matrix, secreting organic acids, inorganic acids, polysaccharides, and other substances that continuously weather the rock matrix by chemical action. For example, mosses form a layer of water on the stone surface after rainfall, increasing the interaction between water and stone [11]. Bacteria are responsible for the formation of biofilms that cause large color changes induced by pigments. By absorbing more light, the temperature change can cause a physical stress through expansion and contraction processes [12, 13]. Some bacterial species, such as sulfur cycle bacteria or ammonia and nitrite cycle bacteria, may be involved in chemical damage to the stone. In sulfur-polluted environments, sulfur cycle bacteria may even convert limestone to gypsum. This gypsum may have a dark coloration caused by airborne particles trapped in extracellular polymeric substance (EPS) [12]. Fungi are also one of the most important microorganisms involved in stone decay.

Black fungi are the most worrisome type of fungi known in stone conservation, because they are ubiquitous, very difficult to remove, and the first recolonizers of a clean stone [14]. Some species, such as the airborne hyphomycetes, can be pioneers of biocolonization, establishing their hyphae in the porous network of the stone [15]. Black fungi also induce bio-pitting and can develop a thin black layer on the surface in association with a lichen. The color is caused by the melanin pigment of the black fungi [14–16]. Fungi can also attack the stone chemically by producing organic acids (oxalic, acetic, citric…) that can degrade stone minerals by solubilizing and chelating [12, 15]. Lichens are mainly involved in the physical attack through the penetration of rhizines composed of fungal filaments and the expansion/contraction of the thallus, which can lift the grain stone surface. As fungi, lichens mainly produce oxalic acid, which causes the formation of calcium oxalate, weddellite and whewellite [12, 15]. These processes take a long time to become significantly visible, but colonization by these microorganisms has been shown to be very rapid.

The alteration of limestone monument occurs at different spatial scales [17]. The changes of stone properties concern the nanoscale and are not visible. The alteration is observable at the microscale (mm to cm) with color change or mass loss, at the mesoscale (cm to m) for different deterioration phenomena and at the macroscale (façade or monument) with structural effects. Microscale and mesoscale alteration can be visible after only a few months of exposure, such as material loss after freeze–thaw action in cold and wet climate [18], such as biocolonization by phototrophic microorganisms and bacteria inducing a greening or a yellowing of the surface [19–21].

It is thus important to understand limestone alteration mechanisms and to determine the associated kinetics as a function of intrinsic and extrinsic parameters to better preserve them. However, all environmental parameters act simultaneously. After long-term exposure (decades or centuries), it is therefore difficult to discriminate the impact of each parameter on the stone deterioration and to assess the synergetic effects. Moreover, the deterioration of limestone monument is not a linear process. One way to understand and quantify the role of a specific parameter is to perform laboratory experiments [9, 22]. Another way is to monitor the first stages of alteration in real conditions.

The aim of this work is therefore to study the first stages of alteration of limestone in terms of biocolonization and weathering. To this end, samples of limestone were exposed for 5 years in different conditions—sheltered and unsheltered from rain and in horizontal and vertical positions—in the Père-Lachaise cemetery (Fig. 1). This site combines the characteristics of an urban area

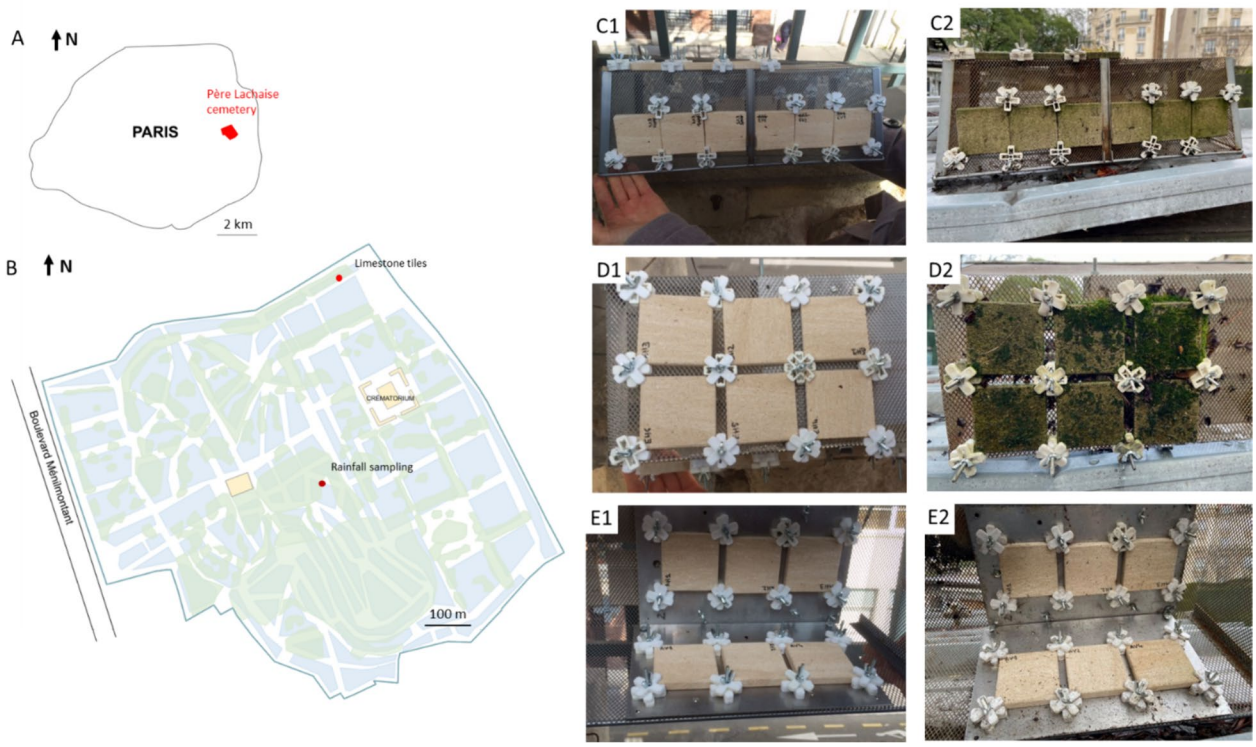

Fig. 1 Site of the study. **A** Location of cemetery in Paris, **B** Map of the cemetery, (C1 to E1) Pictures of the different exposure of the limestone on the rack on the first day of exposure (C1: Exposed Horizontal, D1: Exposed Vertical, E1: Sheltered Horizontal and Vertical); (C2 to E2) Pictures of the different exposure of limestone on the rack after 5 years of exposure (C2: Exposed Horizontal, D2: Exposed Vertical, E2: Sheltered Horizontal and Vertical)

and a heavily planted garden. Moreover, the alteration of ancient tombs has already been studied [23].

Material and methods

Exposure campaign of limestone samples at the Père-Lachaise cemetery

'Saint-Maximin roche fine' limestone is a Lutetian limestone that has been selected for its widespread use in monuments (such as Meaux and Le Mans cathedrals, Saint-Cloud and Vincennes castles…), and as restoration stone for monuments [24]. Moreover, its petrophysical properties are described in the literature [25]. 'Saint Maximin roche fine' limestone is composed of 97% calcite and 3% quartz, with a homogeneous grain distribution. This stone has a porosity of 38% and a water capillary coefficient of $3.7 g.cm^{-2}.h^{-0.5}$.

The Père Lachaise cemetery site was chosen because it is a vegetated area in the center of Paris. This site contains numerous limestone tombs, which may have been altered for up to 200 years. It was interesting to expose pristine limestone in similar conditions. 18 specimens of limestone ($6 \times 6 \times 1$ cm^3) were cut. This size was chosen to perform different analyses and to avoid side effect. The specimens have been then attached to aluminum holders fixed on a metallic structure installed at the Père-Lachaise cemetery in Paris, France (48°51′52.0"N, 2°23′44.2"E) (Fig. 1A, B) from 16 March 2016 to 1 February 2021. 6 specimens were exposed unsheltered from rain and in horizontal position (UH, Fig. 1D), 6 specimens unsheltered from rain and in vertical position (UV, Fig. 1E), 3 specimens in sheltered from rain and in vertical position (SV) and 3 specimens in sheltered and in horizontal position (SH) (Fig. 1F).

The climate in Paris is described as hot temperate (cf. Koppen and Geiger classification) with the presence of rainfall in the driest months. During this period, the annual average temperature was 13.4 °C and the annual average precipitation was 698 $mm{\cdot}a^{-1}$ (MeteoFrance data, Paris Montsouris station).

Before and during the exposure campaign, 2 series of three rainfalls were collected at the Père-Lachaise cemetery. The first one (P1, P2, P3) was sampled between 16 and 27 November 2015 and the second one (P4, P5, P6) from 14 April to 3 May 2016. The sampling site is located in the middle of the Division 25 (see Fig. 1) and is surrounded by tombs and an abundant vegetation with trees

(mainly chestnut, maple, cedar and ash trees) and shrubs. The objective was to collect rainfall samples representative of the site to obtain a range of rain composition to be compared to the composition of the soluble fraction of limestone samples and have a rough assessment of element sources.

Precipitation was sampled using a 24 cm diameter Teflon funnel screwed to a Teflon filter holder fitted with a cellulose acetate filter (0.45 µm porosity and 47 mm diameter) to isolate particulate matter. The system is screwed to a 500 mL polyethylene bottle which collects the filtered rain. Biological development is limited by the prior addition of 100 mg of thymol into the bottle. Two blank samples – one with milliQ® (mQ) water (BL1) and one with mQ and thymol (BL2) – were obtained by using this set-up. After sampling, the pH and the conductivity were measured using a multiparameter analyzer Consort C861 and electrodes. Solutions were stored in a freezer until their analyses by Ion chromatography.

The volume-weighted mean concentration for each period (*VWM* in µeq·L^{-1}) is calculated using:

$$VWM = \sum_{i=1}^{n} C_i P_i / \sum_{i=1}^{n} P_i \quad (1)$$

where C_i is the ionic concentration for each element (in µeq·L^{-1}), P_i the precipitation amount for each rainy event (in mm) and n the total number of rain events. Concentrations of H^+ were calculated from measured pH values. The same equation is used for average pH and conductivity (instead of C_i).

Marine (SW) and crustal (crust) enrichment factors (EFs) correspond to the elemental ratio between ions in rainwater compared to a similar ratio for a reference material. Na^+ can be used as a reference element for seawater and Ca^{2+} for the continental crust. They were calculated to assess the potential sources of major ions in rainwater:

$$EF_{SW} = \left[X/Na^+\right]_{rain} / \left[X/Na^+\right]_{SW} \quad (2)$$

$$EF_{crust} = \left[X/Ca^{2+}\right]_{rain} / \left[X/Ca^{2+}\right]_{crust} \quad (3)$$

With X the concentration of the element of interest in rainwater (in µeq.L^{-1}). Reference ratio are given in [26] for seawater (in µeq.L^{-1}; $Ca^{2+}/Na^+ = 0.044$; $SO_4^{2-}/Na^+ = 0.121$; $Mg^{2+}/Na^+ = 0.227$; $K^+/Na^+ = 0.412$; $Cl^-/Na^+ = 1.161$) and in Rudnick and Gao ([27] for continental crust (in ppm; $Mg^{2+}/Ca^{2+} = 0.613$; $K^+/Ca^{2+} = 0.328$; $SO_4^{2-}/Ca^{2+} = 0.026$).

Samples collection and preparation

After 5 years of exposure, 10 specimens were collected: 3 UH, 3 UV, 2 SV and 2 SH. The remaining 8 specimens will be collected over a longer period (probably 10 years). During the past period, regular observations and measurements of benthic microorganism concentrations (green algae, cyanobacteria and diatoms) by fluorescence using a BenthoTorch (bbe moldaenke®) were carried out. However, the biological development depends on the meteorological conditions during the days preceding the measurement (see S1 in the supplementary material), as confirmed by [28]. Therefore, a 5-year exposure period was chosen to ensure substantial biological colonization and significant changes.

After sampling, for each of the 10 specimens, a sterile swab was used to collect microbial DNA on the limestone surfaces. Then, the limestone surface (first 5 mm) was scratched to collect powder with a sterile scalpel under sterile conditions. The powders from each type of sample (UH, UV, SH and SV) were pooled to perform multiple analyses. In the following, SV_P, SH_P, UV_P, UH_P correspond to the powder scratched from the limestone surface for the three samples and SVi_S (with i from 1 to 3) corresponds to the swab sample for each of the three replicates of limestone in different positions. All the samples were stored in sterile tubes at 4 °C until analyses.

Solid characterization

The surface of the samples was first observed using a digital microscope (Keyence VHX-6000). The samples were also characterized using a tabletop scanning electron microscope (SEM Hitachi TM3030) coupled with energy dispersive X-ray spectrometry (EDS Bruker Quantax 70) to observe the surface change at the microscopic scale and to determine the elemental composition. The technique requires no sample preparation prior to analysis.

In order to identify the crystalline phases present on the limestone surface, XRD analysis was performed on the limestone powder, using a Panalytical Empyrean powder diffractometer equipped with a PIXcel detector fitted with a Cu anode tube (Kα1 = 1.5406 Å) operating at 45 kV and 40 Ma. Crystalline phase identification was performed with QualX and HighScorePlus 2.0 software, using COD and ISDC databases.

Extraction of soluble ions adsorbed on specimens

To extract soluble ions, an elution was performed using 1 g of limestone powder and 9 mL of MilliQ® water (mQ). The solution was placed on a rotator at 40 rpm for 1 h, followed by centrifugation at 14,000*g* for 5 min. The supernatant was collected, filtered at 0.2 µm, and analyzed in triplicate by ion chromatography (IC) to determine the concentrations of cations, anions, and organic acids. Rainfall samples were also analyzed by IC. The instrument is METROHM 930 Compact Flex on the PRAMMICS platform OSU-EFLUVE UMS 3563.

For cations, the eluent is a mix of nitric acid and picolinic acid and a column Metrostep C4 (250 mm, with a mesh of 2.5 µm, Metrohm ®) was used. For anions, the mobile phase is a mix of Na_2CO_3 and $NaHCO_3$ and a column Metrostep A supp 7 (250mm, mesh of 2.5 µm, Metrohm ®) was used. The data processing of chromatograms was carried out using MagIC Net 3.3 software. The limits of quantification are: 1×10^{-5} mg·g^{-1} for magnesium and oxalate; 1.56×10^{-5} mg·g^{-1} for chloride, sulfates and nitrates; 2×10^{-5} mg·g^{-1} for phosphate and fluoride; 2.5×10^{-5} mg·g^{-1} for sodium, potassium, ammonium and calcium; 5×10^{-6} mg·g^{-1} for acetate, propionate and formate.

Biological analyses

Bacterial and fungal estimations have been performed using the Most Probable Number (MPN) method [29]. A part of non-filtered elution (100 µL) was diluted by 10^1, 10^2, 10^3, 10^4 and 10^5. For bacteria, LB broth medium (VWR®) was used, with an addition of fongizone with a concentration of 1g·L^{-1}. For fungi, the medium is Malt extract broth (VWR ®) with addition of ampicillin with a concentration of 1g·L^{-1}. Medium and diluted solutions were introduced in 8 replicates in a microplate. The absorbance was read at 490 nm after 24 h for bacteria and 6 days for fungi. The MPN calculation program used come from [30].

To determine the composition of the limestone microbiome, two types of samples were used for DNA extraction: pooled limestone powder and sterile swabs. DNA was extracted using a DNA extraction Spin Kit for Soil (MPBio ®) according to the manufacturer's instructions. For powder samples (designated _P), 0.5 g of limestone powder was used, and for swab samples (designated _S), the head of the sterile swab was used. Next generation sequencing (library preparation, amplification and sequencing) was performed on the Eurofins Genomics platform using the Illumina MiSeq method on two target regions, ITS1 for fungi and V3-V5 for bacteria.

The bioinformatics treatment was carried out on Galaxy, Migale platform. Databases 16S_SILVA_Pintail100_138 for bacteria and ITS_UNITE_Fungi_8.0 for fungi were used for taxonomic assignment of sequences. Biostatistics including the index of biodiversity (Bray–Curtis beta diversity) were calculated using the Easy16S application, Migale bioinformatics facilities platform.

Statistical analyses

Statistical analyses were performed using RStudio®: non-parametric Kruskal–Wallis test for comparison of samples and post-hoc Conover test (package conover.test), with corrected Bonferroni for the different groups of significance.

Results

Rainfall composition

Six rainfall samples were collected at the Père-Lachaise cemetery: P1, P2, P3 in November 2015 (1st series) and P4, P5, P6 in April 2016 (2nd series) (Table 1). The amount of rain calculated from the collected volume is in agreement with the MeteoFrance data, except for the P2 sample for which the bottle capacity was too low. The pH varies between 4.5 and 6.2 (average 5.4) and the conductivity between 42.9 and 258.0 µS.cm^{-1} (average 119.1 µS.cm^{-1}). A pH of 5.6 corresponds to equilibrium with atmospheric CO_2. Therefore, the rain is acidic for P1, P2, and P4 due to dissolution of NOx or SO_2 in the cloud and raindrops [31, 32]. This is in agreement with the measured pH of precipitation in Europe [33].

Inorganic ions and organic acids were measured for the six samples and the VWM was calculated for the two periods (Table 1). The ion balance can be used to determine the data quality of rainwater samples. For P1-P3 samples, the difference in concentrations between total cations and total anions is less than 11%, which is fully acceptable [34]. For P4-P5-P6, the sum of cations is higher than the sum of anions. However, P6 seems to be contaminated by K^+.

Despite the variability, the range of concentrations for the different elements is comparable to published data (e.g. for northern Europe, [35, 36]). Nevertheless, the sum of cations and anions is higher than published data (~50–200 µeq·L^{-1} for each in [33, 37] vs. 1000 µeq·L^{-1} here).

The main anions are chlorides and sulfates for the 1st series (Nov. 2015) and chlorides, phosphates, sulfates and nitrates for the 2nd series (April 2016). The high phosphate content can be explained by the rainwater sampling conditions. The collector was placed at ground level, close to vegetation and under the tree canopy, since the aim was to sample rainwater that is in contact with the graves. [38] highlighted a high increase in P concentration (by a factor of 6) of the rainwater passing through the tree canopy compared to rainwater falling directly from the atmosphere to the ground. The source of P may be deposited dust or organic matter. This is also consistent with the season, as P6 was collected in the spring. Conversely, the chloride content is lower in the second series. Chloride can be of marine origin, but the enrichment factor for series 1 (between 1.9 and 9.2) is higher than 1 (Table 1). Therefore, chloride can also originate from anthropogenic sources (e.g. biomass burning or road deicing agents [39]), which is also consistent with the season. On the contrary, the EFs for Cl^- in the 2nd series are close to 1, suggesting a marine origin. Sulfates are of anthropogenic origin, as the EFs compared

Table 1 Sampling conditions (dates, volume, amount), pH, conductivity, concentrations in cations, anions and main organic acids (in $\mu eq \cdot L^{-1}$) and calculations of ionic ratio or enrichmentfactors (EF) (Eq. 2 and 3)

		BL1	BL2	P1	P2	P3	VWM	P4	P5	P6	VWM
date from		mQ water	mQ water	2015-11-16 17:00	2015-11-18 09:45	2015-11-23 10:00		2016-04-09 12:00	2016-04-14 16:20	2016-04-24 15:20	
to			+ thymol	2015-1-18 09:45	2015-11-23 10:00	2015-11-27 12:00		2016-04-14 16:20	2016-04-24 15:20	2016-05-03 09:40	
Volume (mL)				75.3	495.4*	465.4		515.58	375.96	241.86	
Amount (mm)				1.7	10.9*	10.3		11.4	8.3	5.3	
Amount (MeteoFrance) (mm)				2.3	35.9	9.9		11.6	8.4	6.1	
pH				5.3	4.5	6.0	4.9	4.9	5.8	6.2	5.4
Conductivity (µS/cm)				148.8	138.6	42.9	118.4	44.7	81.5	258.0	102.4
Calc. conductivity (µS/cm)				93.0	118.1	28.5		24.6	44.0	330.8	
Hydrogen	H^+	0.10	0.10	5.0	31.6	1.0	24.1	13.5	1.7	0.6	6.8
Sodium	Na^+	1.23	0.59	112.1	59.6	72.9	64.3	31.4	59.1	120.6	59.6
Potassium	K^+	1.04	1.71	240.2	301.1	48.5	244.6	27.8	98.1	1337.1***	57.5***
Calcium	Ca^{2+}	< LD	< LD	367.2	282.4	42.1	233.8	23.0	76.0	275.3	94.4
Magnesium	Mg^{2+}	< LD	< LD	98.7	123.9	18.8	100.4	10.0	23.9	194.7	54.0
Ammonium	NH_4^+	< LD	0.99	74.8	11.8	23.6	16.5	65.3	98.8	389.1	145.5
Chloride	Cl^-	0.86	0.76	785.0	634.9	158.3	537.7	40.6	76.0	213.0	89.1
Sulfate	SO_4^{2-}	5.47	0.34	90.0	73.0	28.9	64.1	23.5	51.0	150.2	59.7
Nitrate	NO_3^-	< LD	0.89	52.7	11.9	15.6	14.1	40.3	85.5	5.7	47.9
Phosphate	PO_4^{2-}	44.18	0.43	6.2	0.0	0.0	0.2	1.9	25.8	373.6	89.2
Fluoride	F^-	< LD	< LD	2.1	1.4	0.3	1.2	< LD	1.1	9.3	2.3
Bromide	Br^-	< LD	0.37	0.51	0.49	0.23	0.4	< LD	< LD	0.8	0.2
Acetate	CH_3COO^-	0.47	0.71	10.1	0.4	0.0	0.7	1.5	1.6	139.5	31.0
Propionate	$C_2H_5COO^-$	< LD	< LD	1.1	0.0	0.0	0.0	0.1	0.1	1.5	0.4
Formate	$HCOO^-$	0.13	0.27	13.2	0.1	0.1	0.6	0.7	0.8	73.5	16.3
MSA	$CH_3SO_3^-$	< LD	< LD	0.5	0.0	0.0	0.0	0.1	0.4	< LD	0.2
Oxalate	$C_2O_4^{2-}$	< LD	0.09	3.2	4.6	0.1	3.6	0.9	0.6	19.2	4.7
Σ cations		2.38	3.39	898.1	810.5	206.8	683.8	170.9	357.7	2317.5	417.9
Σ anions		51.1	3.9	964.5	726.8	203.6	622.8	109.6	242.9	986.3	340.9
Ion difference		− 182%	− 13%	− 7%	11%	2%	9%	44%	38%	81%	20%
Σ organic acids		0.6	1.1	28.0	5.1	0.3	4.9	3.3	3.6	233.7	52.5
Σ total		53.5	7.2	1862.6	1537.3	410.3	1306.5	280.6	600.6	3303.9	758.8
$SO_4^{2-} + NO_3^-$ / $Ca^{2+} + Mg^{2+}$				0.31	0.21	0.73	0.23	1.93	1.37	0.33	0.72
EF SW K				97.4	229.5	30.3	172.8	40.4	75.4	503.9	43.8
EF SW Ca				74.5	107.6	13.1	82.6	16.7	29.2	51.9	36.0
EF SW Mg				3.9	9.2	1.1	6.9	1.4	1.8	7.1	4.0

Table 1 (continued)

	BL1	BL2	P1	P2	P3	VWM	P4	P5	P6	VWM
EF SW SO4			6.6	10.1	3.3	8.2	6.2	7.1	10.3	8.3
EF SW Cl			6.0	9.2	1.9	7.2	1.1	1.1	1.5	1.3
EF Crust K			2.0	3.3	3.5	3.2	3.7	3.9		1.9
EF Crust Mg			0.5	0.9	0.9	0.9	0.9	0.6	1.4	1.2
EF Crust SO_4			9.3	9.8	36.2	14.4	53.7	35.3	28.7	33.3

The amount of rain is calculated from the volume and compared to MeteoFrance data (Montsouris and Saint-Antoine stations). The conductivity was directly measured and calculated from concentrations and molar ionic conductivity values for comparison. The volume-weighted mean (VWM) are calculated using Eq. (1)

*The volume and the amount of rain during this period are underestimated because the bottle had a capacity of 500 mL while the amount of rain was higher

**Calculations are based on Meteofrance rainfall for P2 sample

***There is a probable contamination for this K concentration and it was not taken into account in the calculation of the VN

to seawater and continental crust are mostly higher than 1. They can come from the combustion of sulfur-containing fuels. Nitrates also come from industrial activities and transportation.

The main cations detected are calcium, potassium, magnesium, sodium and ammonium (Fig. 2). Calcium and sodium are assumed to originate mainly from the continental crust and seawater, respectively, and are used as reference for the calculation of the EFs (Eqs. 2 and 3). For Mg^{2+}, EF_{SW} is close to or greater than 1, indicating additional sources to the marine salts, while EF_{crust} is slightly less than 1. Thus, Mg^{2+} is certainly of natural origin. For K^+, EF_{SW} is much higher than 1 (30 to 500), highlighting additional sources to the marine salts, while EF_{crust} is slightly higher (2 to 4). K^+ could originate from biomass burning, but, except for P6, K^+ is very well correlated with Ca^{2+} and Mg^{2+}, and not with NH_4^+ or phosphates (not shown).

The acidity is mainly due to sulfuric acid and nitric acid and neutralization by Ca^{2+} and Mg^{2+} [37, 40]. Thus, the ratio $(SO_4^{2-}+NO_3^{2-})/(Ca^{2+}+Mg^{2+})$ was calculated. Since the main anion is Cl^-, the ratio is less than 1 (0.23 and 0.72, Table 1). This shows the alkaline nature of the rainwater.

The concentrations of organic acids are relatively low. The main ions analyzed are formate, acetate and oxalate, which is in agreement with other studies [41]. Their sources can be direct (biogenic emissions, biomass burning) or secondary (photochemical oxidation of precursors from natural and anthrogenic sources) [42].

The comparison of the three samples of each series shows a variability. For the first series, the concentrations tend to decrease with time (Table 1), especially for Ca^{2+}, Cl^-, SO_4^{2-}, F^-, Br^-. Except for oxalate, the organic acids are high in P1 and close to the detection limits for P2 and P3. There is an increase between P1 and P2 and then a decrease in P3 for K^+ and Mg^{2+}. An opposite trend is observed for Na^+, NH_4^+ and NO_3^-. In terms of enrichment factors, P3 is closer to P4 and P5. For the 2nd series, there is a general increase in concentrations, except for nitrates, which are low for P6. These changes in the ionic concentration indicate that the soluble components in the air are scavenged by the leaching process.

Even if the variability of the rainfall is high according to the season or to the scavenging rate, the results give a range of typical concentrations of rainwater (compared to other studies) that could be used for controlled alteration experiments in laboratory and as a reference to compare with the soluble fraction of limestone samples. It is also shown that the local effect of the vegetation can influence the phosphate concentration.

Weathering observations

After 5 years of exposure, a greenish patina is visible on exposed limestone specimens (UV and UH) (Fig. 3A, B). Significant moss development is also observed on UH specimens (Fig. 3B). Sheltered specimens (SH and SV) do not show the presence of patina, but rather a gray coloration. The presence of green spherical structures on UV (Fig. 3B) and UH (Fig. 3C) can be assimilated to green algae. On UH, the moss development with small leaves is clearly visible (Fig. 3C). In sheltered positions (SH and SV) some fungal hyphae are visible (Fig. 3E).

SEM analysis was performed on each specimen (Fig. 4). Qualitative observations were made, but no significant neocrystallization was observed. Also, specimens with a lot of organic matter, such as UV, were not observed.

Crystalline phases analysis

XRD analyses (Fig. 4) show two major phases: calcite and quartz for all positions and unweathered limestone (CS). For the sheltered positions SH and SV, KNO_3 was also detected with peaks around 26° (2-theta) Potassium nitrate is also known as saltpeter or niter. The main source is usually natural fertilizers (Fig. 5).

Results of the elution analyzed by ion chromatography

The results of limestone elution are shown in Table 2 and Fig. 6. The elements can come from the substrate weathering (dissolution, secondary phases within the porous network or at the surface) or from wet or dry deposition. The obtained concentrations of Mg^{2+}, Cl^- and F^- are very low. These elements are either poorly soluble such as Mg in carbonates, or poorly concentrated as exogenous elements in limestone (Cl and F), while they can be present in rainwater (Table 1). For the other elements, there is an increase in the concentrations of all components compared to the original limestone. However, there are differences depending on the situation and position. The concentrations of Na^+, K^+, NH_4^+, PO_4^{3-} and organic acids (except for formate) are higher in unsheltered samples. Since they are exposed to rain, they can be soaked by these elements. On the contrary, the concentrations in the sheltered samples are higher for Ca^{2+} and NO_3^- (with a factor of 2 for Ca^{2+} between sheltered and unsheltered position; factor of 3 to 5 for NO_3^-) and relatively similar for SO_4^{2-}. Ca is one of the major constituents of limestone. Elution of pristine limestone leads to a significant release of this element. Under sheltered conditions, an additional source may be provided by exogenous particles or slight dissolution of calcite or neoformed gypsum. Nitrates and sulfates are of atmospheric origin and can accumulate on the surface without regular leaching.

The comparison between the orientations shows that in the sheltered condition, the highest concentrations are

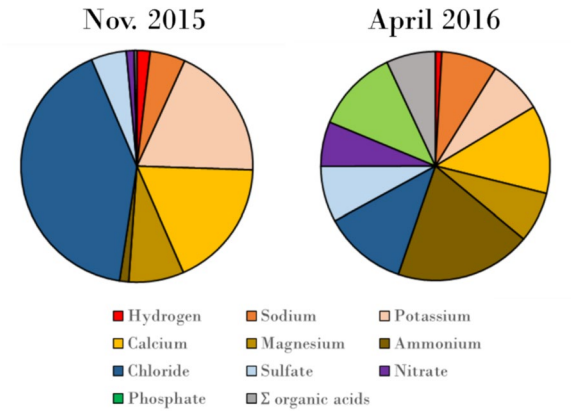

Fig. 2 Respective contribution (in %) of the volume-weighted mean concentrations of the main elements of the rain for the 2 series (Nov. 2015 and April 2016)

measured in the vertical position for all mineral elements (Na^+, K^+, SO_4^{2-}, NO_3^-) and for oxalate, whereas the concentrations of other organic acids are very low in the vertical position. Dry deposition is probably easier in the vertical position than in the inverted horizontal position. The concentrations of organic acids are surprisingly low for SV samples. In unsheltered conditions, the concentrations are higher in the vertical position only for Na^+ and oxalate. They are significantly higher in horizontal position for SO_4^{2-} and PO_4^{2-} and other organic acids and relatively close for K^+, Ca^{2+}, NH_4^+. For phosphates and organic acids, this may be related to the growth of moss on the surface of horizontal samples.

Microbial enumeration

Enumeration using the Most Probable Number (MPN) technique gives a good estimate of the number of heterotrophic cultivable bacteria and fungi. The values for the exposed positions UH and UV (Fig. 6) are 2 or 3 orders of magnitude higher than those for the sheltered positions. The difference is more important for bacteria (Fig. 6A) than for fungi (Fig. 6B), since the number of bacteria after 24 h in the sheltered position is very low (< 10 cells/0.5 g of limestone). For the exposed positions, the number of bacteria is higher in the horizontal position than in the position, while the number of fungi is lower.

Identification of *phyla*

The sequencing results allowed to calculate the relative abundance of the different phyla for bacteria and fungi (Fig. 7). The bacterial communities on the samples belong to eight main phyla (Fig. 7A). The most abundant are Proteobacteria (25–65%), Deinococcota (2–15%), Cyanobacteria (5–30%), Bacteroidota (2–55%) and Actinobacteriota (7–55%). These five phyla are present in all the samples but not in the same proportions.

The percentage of Actinobacteria is higher in the sheltered position (31% for SH and 53% for SV) than in the exposed position (values ranging between 7 and 18% for UH and 18 and 26% for UV). Bacteroidota are

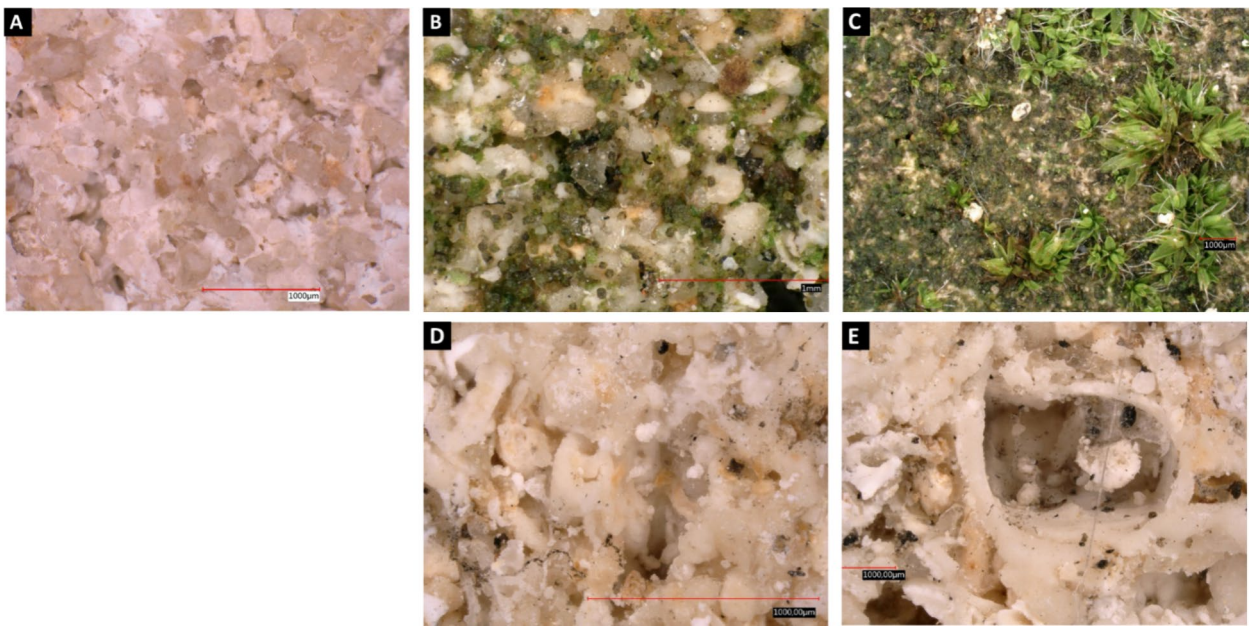

Fig. 3 Microscopic observation of limestone specimens after 5 years exposure in Père-Lachaise cemetery **A** Pristine limestone, **B** Unsheltered Vertical (UV), **C** Unsheltered Horizontal (UH), **D** Sheltered Horizontal (SH), **E** Sheltered Vertical (SV)

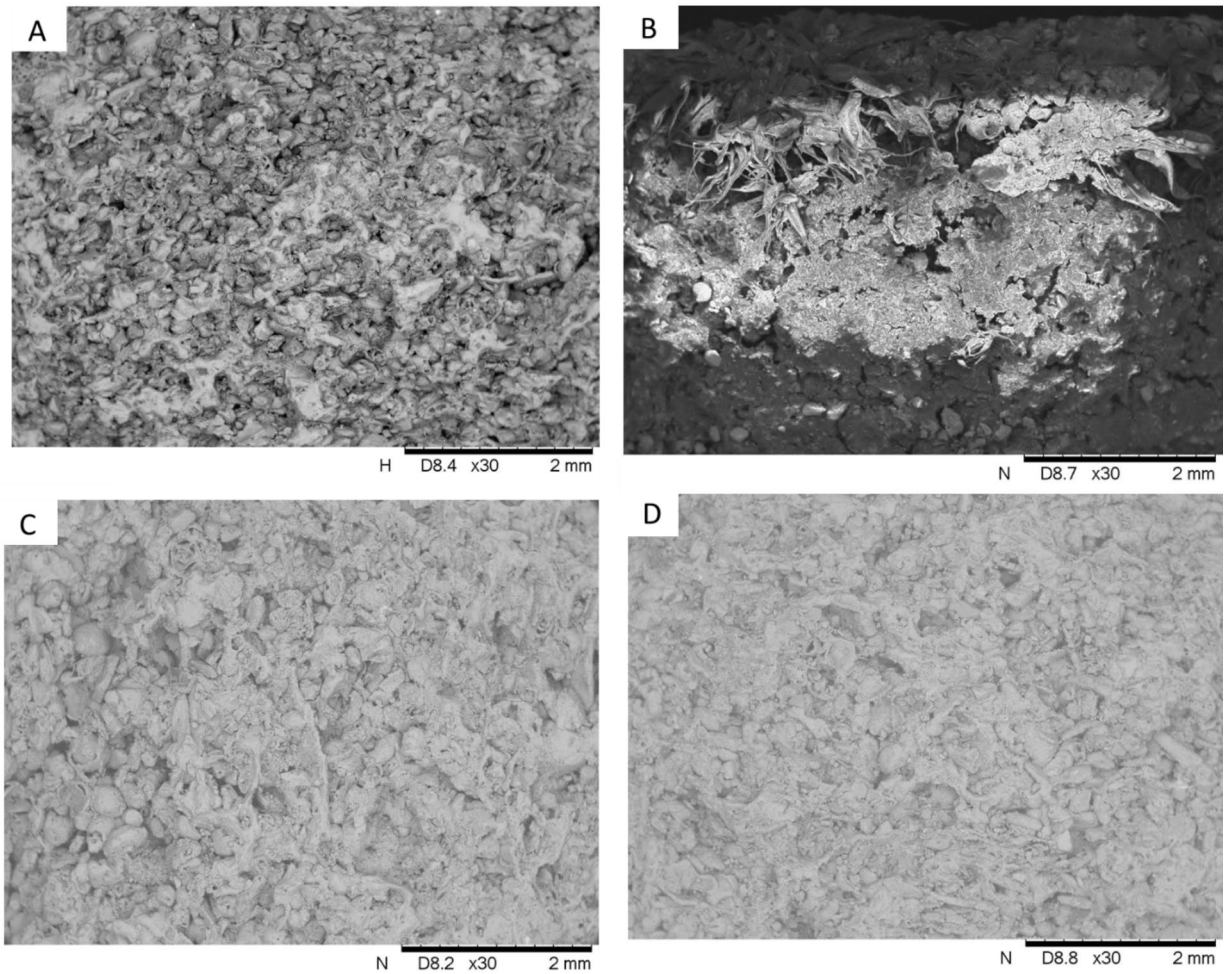

Fig. 4 SEM observation of limestone specimens after 5 years of exposure at Père Lachaise. **A** Pristine limestone (no exposure), **B** Unsheltered Horizontal (UH), **C** Sheltered Vertical, **D** Sheltered Horizontal (SH)

more abundant in the horizontal position (28% for SH and 8–58% for UH) than in the vertical position (8.7% for SV and 2–6% for UV), regardless of exposure. The abundance of Deinococcota is higher in the UH position, with a relative abundance of 6.4–14%, while the values for the other positions are less than 3%. The relative abundance of Proteobacteria is higher on the UV sample, with values ranging between 44 and 63%, than on the other positions, where the relative abundance is less than 30%.

The fungal communities are composed of 2 main phyla, Ascomycota and Basidiomycota (Fig. 7B). A significant fraction is unidentified for exposed positions (between 5 and 20%), which may be due to the sequencing of some algae that are not recognized with the fungal database used in this study. Ascomycota is the most abundant phylum (> 90% for SH, SV and UH, ~ 75% for UV). Thus, less than 10% of the communities are composed of Basidiomycota, this phylum being more abundant on UH and UV (5–20%).

Bacterial diversity at the genus level

Bacterial diversity can be detailed at different taxonomic levels, sometimes down to genus level (Fig. 8). Irrespective of the sampling positions (UH, UV, SH, SV), the same 5 phyla were found to represent more than 60% of the bacterial diversity: Actinobacteria, Bacteroidota, Cyanobacteria, Deinococcota and Proteobacteria.

The phylum Actinobacteria is mainly represented by the genera *Friedmanniella*, *Nocardioides* and *Marmoricola*. These genera are found in all the positions, but not in the same proportions. For the genus *Friedmaniella*, the relative abundances are higher in sheltered positions (with 10% for SH and 11% for SV) than in exposed positions, where the relative abundance ranges between 0.3 and 1% for UH and between 1.7 and 3.4% for UV.

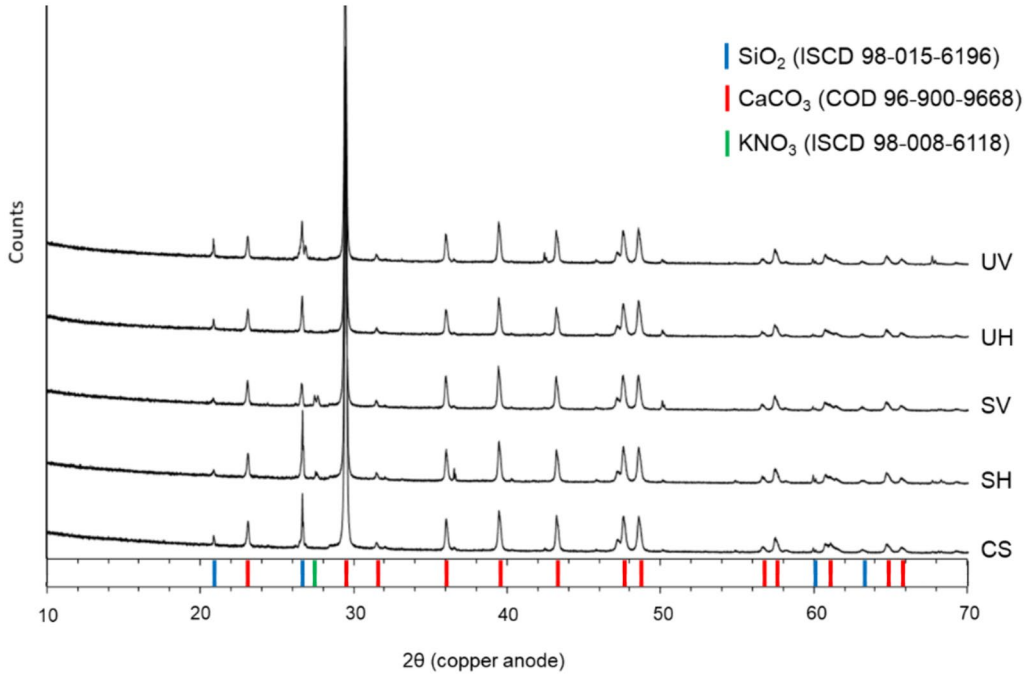

Fig. 5 XRD analysis of pristine (CS) and weathered conditions (SH, SV, UH, UV); the red reference corresponds to calcite (CaCO3, COD 96-900-9668), the blue one to quartz (SiO2, ISCD 98-015-6196) and the green one to KNO3 (ISCD 98-008-6118))

Table 2 Soluble ions concentration (in $mg.g^{-1}$) in elution solution after immersion in mQ water for 24 h of pristine (CS) and weathered (SH, SV, UH, UV) samples

Sample	CS	SH	SV	UH	UV
Sodium	0.017 ± 0.000^{c}	0.152 ± 0.001^{a}	0.279 ± 0.001^{b}	0.967 ± 0.005^{d}	1.577 ± 0.015^{e}
Potassium	0.012 ± 0.000^{c}	0.044 ± 0.001^{a}	0.107 ± 0.002^{b}	0.557 ± 0.003^{d}	0.595 ± 0.000^{e}
Calcium	0.364 ± 0.003^{c}	1.091 ± 0.006^{a}	1.342 ± 0.004^{b}	0.579 ± 0.011^{d}	0.457 ± 0.006^{e}
Magnesium	0.022 ± 0.001^{b}	0.029 ± 0.002^{a}	0.027 ± 0.002^{a}	0.038 ± 0.002^{c}	0.034 ± 0.000^{c}
Ammonium	$< LQ^{b}$	0.005 ± 0.001^{a}	$< LQ^{b}$	0.469 ± 0.008^{c}	0.582 ± 0.005^{d}
Chloride	0.004 ± 0.000^{c}	0.053 ± 0.000^{a}	0.092 ± 0.000^{b}	0.061 ± 0.004^{d}	0.055 ± 0.000^{e}
Sulfate	0.023 ± 0.001^{c}	1.600 ± 0.001^{a}	2.761 ± 0.012^{b}	3.599 ± 0.022^{d}	2.468 ± 0.025^{e}
Nitrate	0.004 ± 0.000^{b}	0.188 ± 0.002^{a}	0.302 ± 0.001^{a}	0.063 ± 0.010^{c}	0.064 ± 0.001^{c}
Phosphate	$< LQ^{c}$	0.017 ± 0.006^{a}	0.003 ± 0.001^{b}	1.726 ± 0.016^{d}	0.367 ± 0.003^{e}
Fluoride	0.038 ± 0.000^{c}	0.006 ± 0.000^{a}	0.006 ± 0.000^{b}	0.005 ± 0.000^{d}	0.005 ± 0.000^{e}
Acetate	0.002 ± 0.000^{c}	0.014 ± 0.002^{a}	$< LQ^{b}$	0.067 ± 0.000^{d}	0.045 ± 0.004^{e}
Propionate	0.000 ± 0.000^{b}	0.004 ± 0.000^{a}	$< LQ^{b}$	0.031 ± 0.000^{c}	0.022 ± 0.001^{ac}
Formate	0.001 ± 0.000^{c}	0.014 ± 0.001^{a}	$< LQ^{b}$	0.020 ± 0.001^{d}	0.009 ± 0.001^{e}
Oxalate	$< LQ^{c}$	0.015 ± 0.000^{a}	0.017 ± 0.000^{b}	0.023 ± 0.002^{d}	0.029 ± 0.001^{e}

The letters a,b,c,d, and e represent the significant difference on ion concentration as a function of the position after Kruskal–Wallis to compare samples and Conover tests corrected Bonferroni for the difference groups of significances. < LQ means inferior of limit of quantification

Nocardioides is mainly present on SV (with an abundance of 11%), followed by SH (5.3%). On exposed samples, *Nocardioides* is more abundant on UV (between 3 and 8%) than on UH samples (2–4%). This genus seems to be more abundant on vertical orientation than on horizontal one. Then, the genus *Marmoricola* is present in greater abundance on the SV sample (7.3%). On the other samples (SH, UH and UV), this genus represents less than 3% of the genus present. Actinobacteriota are more present on the sheltered than on the exposed positions and seem to be sensitive to this parameter.

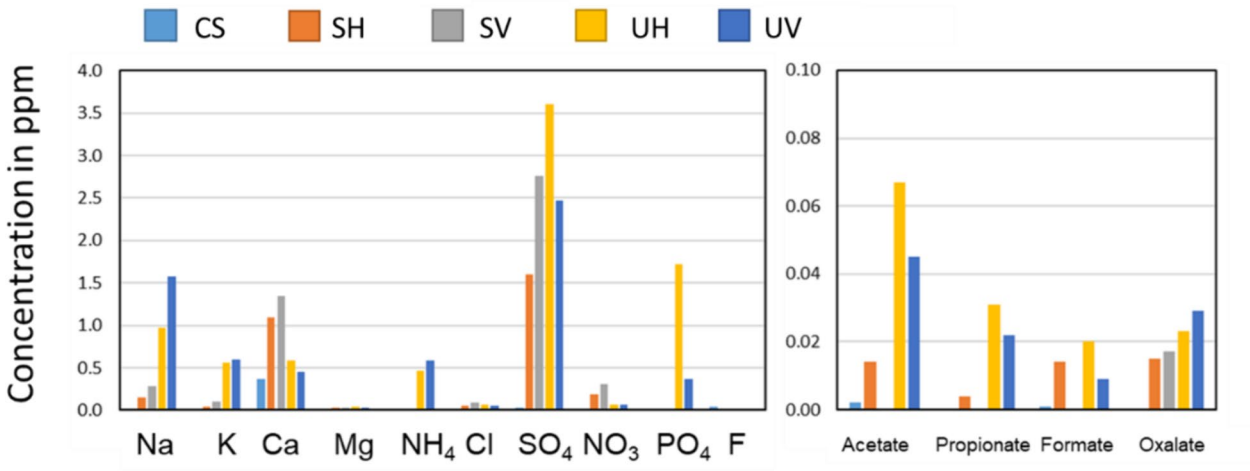

Fig. 6 Concentrations (in ppm) in elution solution after immersion in mQ water for 24 h of pristine (CS) and weathered (SH, SV, UH, UV) samples

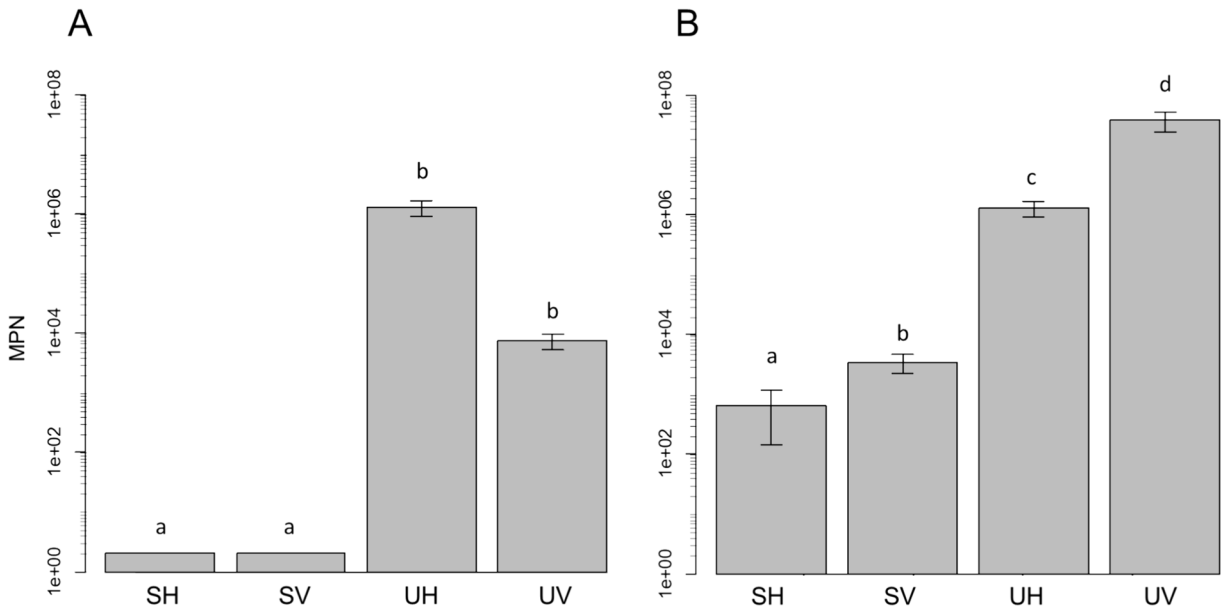

Fig. 7 Enumeration of bacteria (**A**) and fungi (**B**) in cells.mL^{-1}. Letters a, b, c and d represent the similarity degree after statistical Kruskal Wallis test to compare samples and the post hoc Conover test corrected Bonferroni to the difference groups of significance

The horizontal or vertical orientation does not seem to influence their development.

Bacteroidota are mainly represented by the genus *Flavobacterium*. This genus is abundant on SH and UH (21.4% and between 5 and 50%, respectively). On the vertical positions SV and UV, the relative abundance of this genus represents less than 3% of the samples.

Cyanobacteria represent 5–30% of the bacterial abundance at the phyla level. Cyanobacterial sequences are difficult to relate to the genus level for the sequencing study region, therefore only two genera of cyanobacteria are identified: *Nostoc* and *Scytonema*. The abundances of these two genera are less than 1%.

The phylum Deinococcota is mainly represented by the genus *Truepera*. Its relative abundance is higher in the UV position (between 6.5 and 14%) than in the other samples (< 2.5%).

Finally, the Proteobacteria phylum is mainly represented by the genera *Roseomonas*, *Methylobacterium-Methylorubrum*, *Rubellimicrobium*, *Sphingorhabus* and

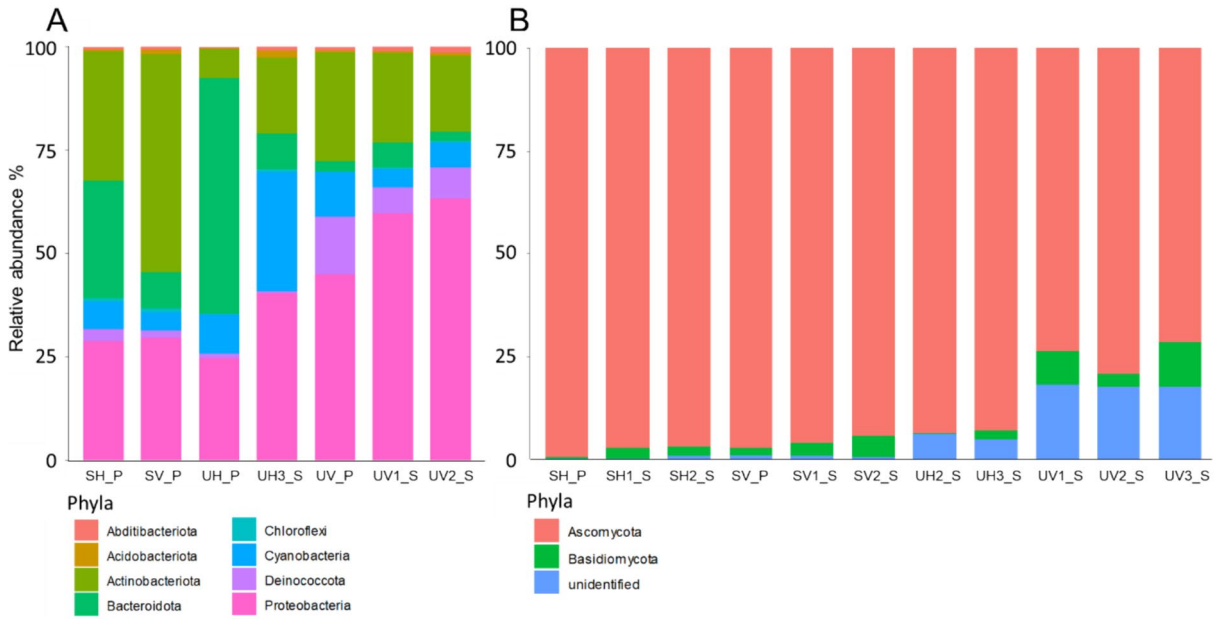

Fig. 8 Relative abundance (in %) of phyla of bacterial (**A**) and fungal communities (**B**) for the different weathered samples (SH, SV, UH, UV) by using the powder (_P) or the swab (_S) methods. Different samplings were performed for the swab method

Sphingomonas. *Methylobacterium-Methylorubrum* and *Sphingomonas* genera have the same behavior with their highest abundance on UV, ranging (between 7–22% and 22–38%, respectively). For *Methylobacterium-Methylorubrum*, the relative abundances are 7.7% for SV, 4.9 for SH and range between 1.5 and 3.6% for UH. For *Sphingomonas,* the relative abundance is 5% for SH and UH, and 6.5% for SV. The values for *Roseomonas* are higher in the vertical positions SV and UV (5.8% and 1.7–5%, respectively). For SH and UH, the relative abundances are less than 3%. The highest abundance of the genus *Sphingorhabus* is on the UH position (3–12%), followed by the SH position (1.2%). This genus is absent on SV and UV positions.

Fungal communities on genus level

The phylum Ascomycota represents between 75 and 98% of the fungi present on the samples. Regardless of the position, three dominant classes were found: Dothiedomycetes, Eurotiomycetes and Lecanoromycetes (Figs. 9 and 10).

The proportion of Dothiedomycetes is higher on the sheltered positions (91–93% for SH and 84–86% for SV) than on the exposed positions (32–59% for UH and 15–20% for UV). On the contrary, the proportion of Eurotiomycetes is higher on the exposed (6–22% for UH and 24–38% for UV) than on the sheltered positions (0.6–1.2% for SH and 1.2–4.8% for SV). Lecanoromycetes show a similar trend with higher relative abundances for UH and UV (18–25% and 1.4–27%, respectively) than for SH and SV (< 0.4%).

The class Dothiedomycetes is mainly represented by 4 genera: *Cladosporium*, *Ramularia*, *Aureobasidium* and *Macroventura*. Regardless of the sampling method, the relative abundances of *Cladosporium*, *Ramularia* and *Aureobasidium* are higher in the sheltered position SH and SV than in the exposed position UH and UV. For *Cladosporium*, the relative abundance ranges between 54 and 65% for SH and between 22 and 35% for SV, while it is below 1% for UH and UV. For *Ramularia*, the relative abundance ranges between 18 and 23% for SH and between 13 and 43% for SV, while this genus is absent on the exposed position. Finally, for *Aureobasidium*, the relative abundance is 4–9% for SH and 4–18% for SV, where it is less than 1% on the exposed position. In contrast to the previous genera, the relative abundance of *Macroventura* is higher for UH (4–19%) and UV (0.6–3%) than for SH and SV (< 1.5%).

The taxonomical assignment up tol genus level is not very accurate for the class Eurotiodomycetes. The orders Chaetothyriales and Verrucariales have the highest relative abundance of this class and are higher on the exposed (UH and UV) than on the sheltered positions (< 1% for SH and SV). Chaetothyriales are more abundant on UV (18–24%) than on UH (0.5–3%). In contrast, Verrucariales are more important

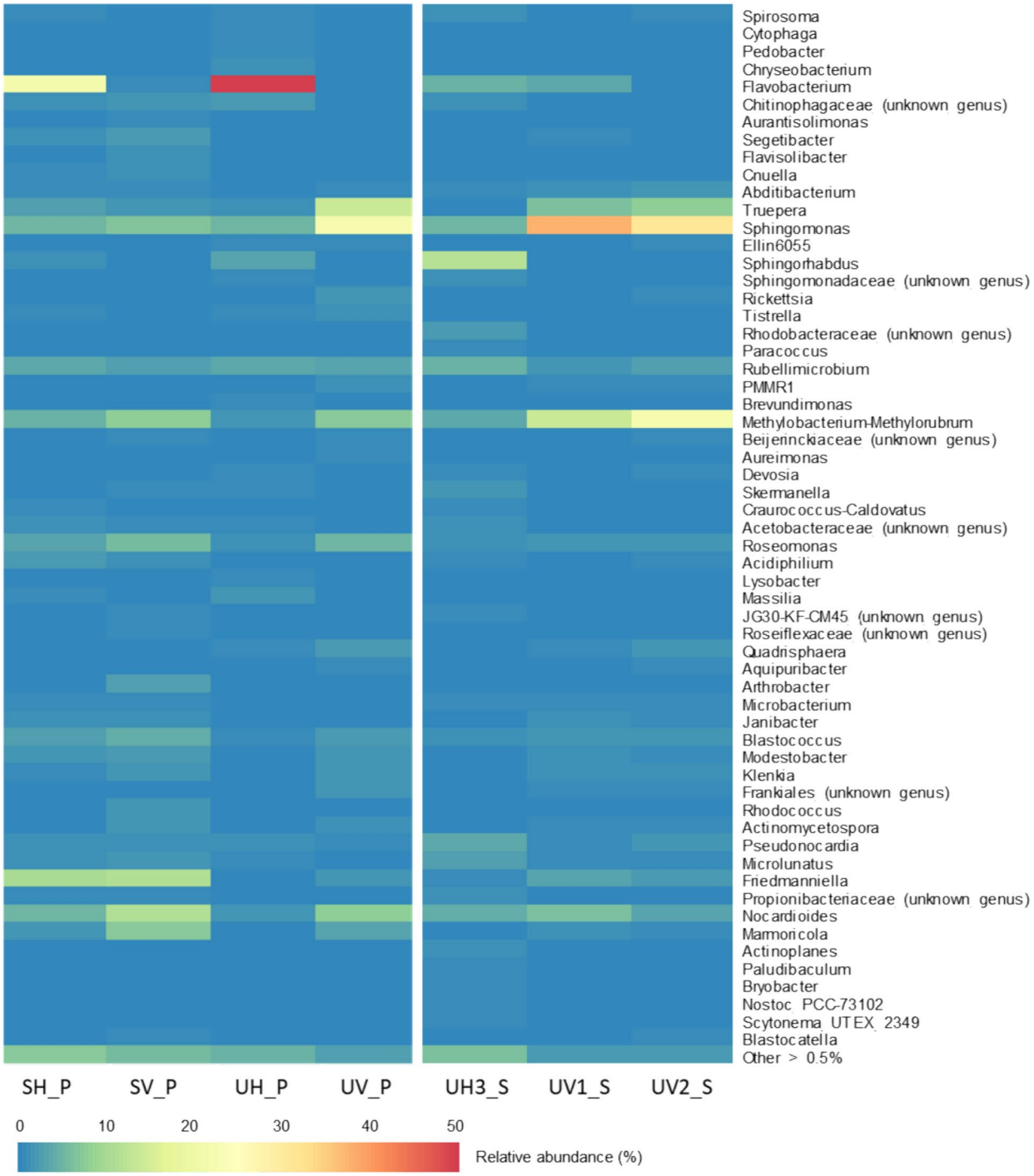

Fig. 9 Heat map representing the relative abundance (in %) of bacteria at genus level for each sample (SH, SV, UH, UV) collected either as powder (_P) or with a swab (_S). Only genera represented have relative abundance superior to 0.5%

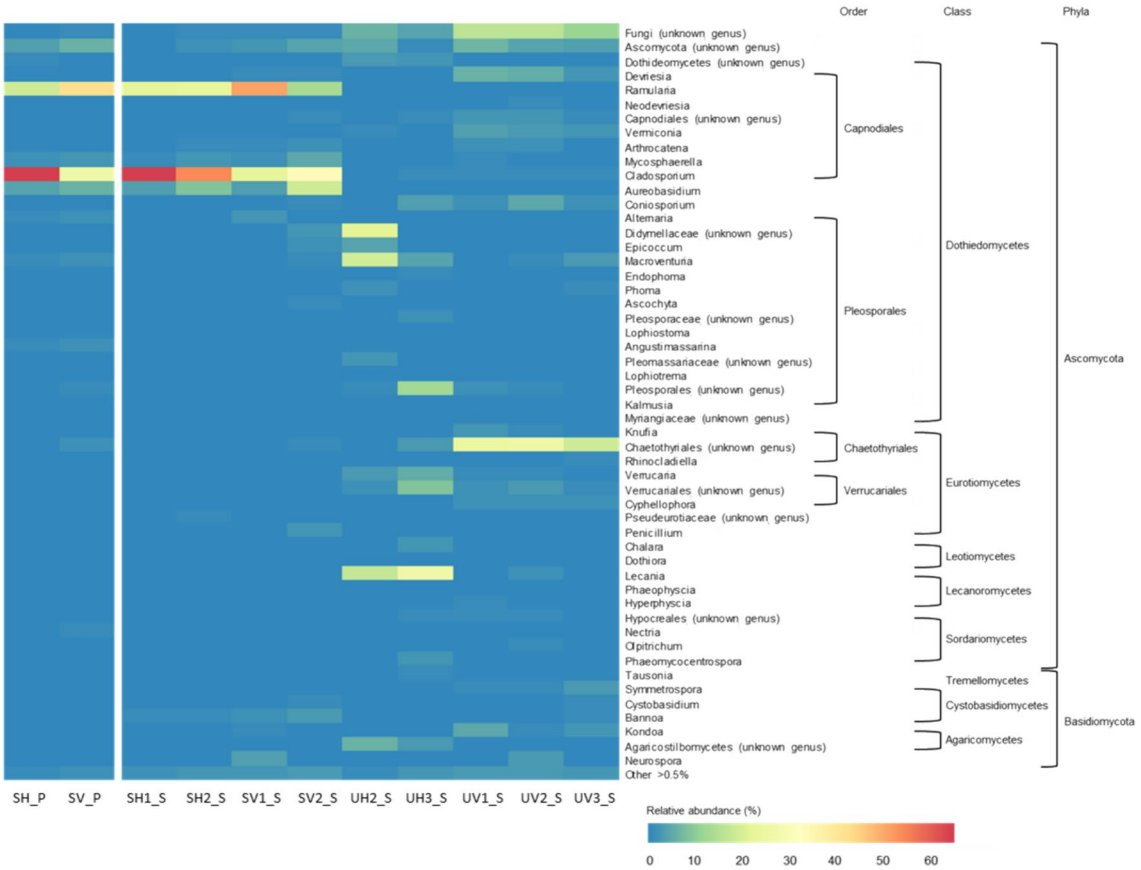

Fig. 10 Heatmap showing the relative abundance of the most represented fungi in each position at genus level. Genera represented have relative abundance superior to 0.5%

on UH (1–9%) than on UV (1–3%). The genus *Verrucaria* follows the same trend with the highest relative abundance on UH, (3–6% depending on the sampling method).

The genus *Lecania,* representing Lecanoromycetes on samples, is mainly present on exposed positions (17–25% for UH and 0.5–15% for UV) and sparse on sheltered positions (< 1%).

Dissimilarity of microbial community: Bray–Curtis *beta* diversity index

Comparison of sampling methods

Two sampling methods were used for DNA extraction. In order to compare the 2 sampling methods, the Bray Curtis beta diversity was calculated (Table 3). This index allows the comparison of the composition of two samples at the species level. For bacteria, the sequencing was possible for both UH and UV sampling methods. For fungi,

Table 3 Bray–Curtis beta diversity indices of bacteria and fungi as a function of the position and exposure condition

Bacteria		**UH_P**	**UH3_S**		**UV_P**	**UV1_S**	**UV2_S**
	UH_P	0	0.6	UV_P	0	0.39	0.4
	UH3_S		0	UV1_S		0	0.3
				UV2_S			0
Fungi		**SH_P**	**SH1_S**	**SH2_S**	**SV_P**	**SV1_S**	**SV2_S**
	SH_P	0	0.16	0.24	SV_P	0	0.25	0.43
	SH1_S		0	0.27	SV1_S		0	0.51
	SH2_S			0	SV2_S			0

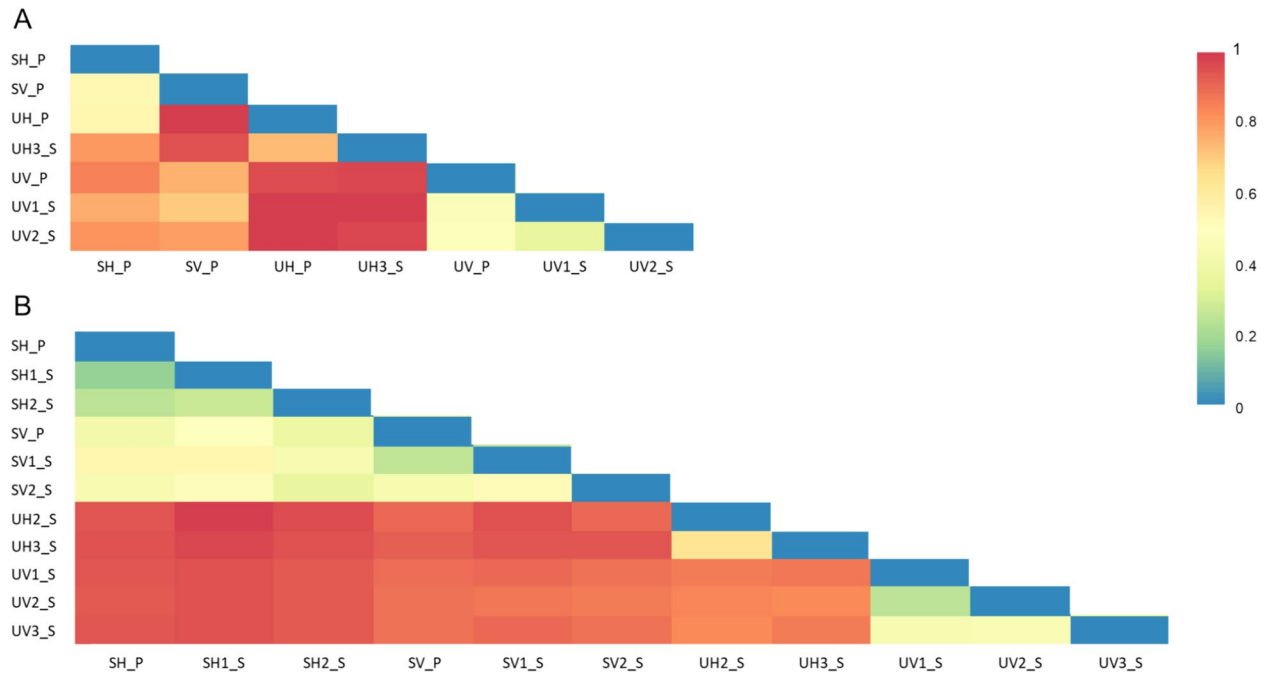

Fig. 11 Heat map showing the Bray Curtis beta diversity index for bacterial communities (**A**) and fungi communities (**B**). Beta diversity index of 1 correspond to a high dissimilarity and 0 correspond to a high similarity

the comparison was possible for samples SH and SV. The result of the Bray Curtis beta diversity is shown in Table 3. The dissimilarity of the microbial communities as a function of the sampling method shows low values, between 0.1 and 0.5, for bacteria and fungi. Therefore, it is possible to have different positions without taking into account the sampling method.

Comparison of the positions

For bacteria (Fig. 11A), the comparison of the sheltered positions SH-SV with the exposed positions UH – UV shows a high dissimilarity (beta diversity ~ 0.7–0.8), except for SH-UH (~ 0.5). This low value can be explained by the important abundance of *Flavobacterium* in the horizontal position (Fig. 8). The beta diversity between horizontal and vertical position is low for sheltered position, indicating a relative similarity, whereas it is high for exposed positions (0.9–1), corresponding to high differences. For fungi (Fig. 11B), the differences between sheltered and unsheltered positions are high (beta diversity between 0.9–1). Fungal diversity is relatively similar between sheltered horizontal and vertical positions (SH-SV) with values between 0.4 and 0.5, but very different between exposed horizontal and vertical positions (UH and UV) with very high with values around 0.8.

Discussion

The aim of this study was to understand the first steps of colonization of limestone in an urban area, in different positions (sheltered or unsheltered) and orientations (vertical or horizontal).

Biocolonization

After 5 years of exposure, the difference in biocolonization is clearly observed on limestone. The biological colonization is higher on the surfaces exposed to rain than on the sheltered surfaces and appears as a green patina induced by photolithotrophic microorganisms and moss development. This greenish patina is often found on limestone monuments after a long period of exposure [13, 43, 44]. This orientation allows a higher water availability due to the contact with rain and a more important solar radiation, in contrast to sheltered samples (SH and SV).

The sequencing results highlight the presence of five major bacterial phyla: Actinobacteria, Bacteroidota, Chloroflexi, Deinococcota and Proteobacteria. These phyla are commonly found on limestone monuments [23, 45–47]. Proteobacteria and Actinobacteria are often dominant in epilithic communities [48–50]. The most important bacterial genera found are *Flavobacterium*, *Truepera*, *Sphingomonas*,

Methylobacterium-Methylorubrum, *Roseomonas*, *Friedmaniella*, *Nocardioides* and *Marmoricola*. Their proportion varies according to their position of exposure. The genus *Sphingomonas* is often present on stone monuments, regardless of the type of stone. They are known to be able to produce a yellow pigment that they use as a sunscreen, allowing them to survive under high UV irradiation. This may explain their higher proportion on exposed vertical positions [47, 50–52]. The genus *Methylobacterium-Methylorubrum* is known to produce carotenoid pigments and has previously been found in bacterial communities associated with stone monuments [47, 50, 53]. The genus Flavobacterium from the phylum Bacteroidetes is present in large proportions in horizontal positions. This genus has been found in very advanced bioalteration facies in both vertical and horizontal positions [54, 55]. This may be due to the greater amount of water retained in some areas, as this genus is commonly found in aquatic systems [56].

The fungal communities are mainly composed of two phyla, Ascomycota and Basidiomycota. The main genera found on limestone surfaces are *Ramularia*, *Cladosporium*, *Aureobasidium*, *Lecania* and their abundance depends on their position. The genera *Aureobasidium* and *Cladosporium* are found in high abundance on the sheltered positions, in agreement with other short-term exposure studies [57]. These genera are common airborne fungi, corresponding to black fungi and act as first fungal colonizers in humid to temperate climates [14–16, 58].

The effect of the orientation (vertical or horizontal) on the microbial communities is clearly observed only for samples exposed to rain, with high values of beta diversity for bacteria and fungi, in contrast to sheltered samples. This can also be explained by the difference availability of water. In the exposed position, where the presence of photolithotrophic microorganisms is higher, the most abundant fungi are considered to be lichenized fungi, such as the genus *Lecania*, the families Verrucariales and Chaetothyriales [59].

Therefore, the microbial communities are relatively similar for short- and long-term exposed stones, suggesting that they are dependent on environmental conditions rather than the state of alteration of the substrate. This suggestion is strengthened by the strong influence of the orientation of the samples, which can be explained by water availability, but possibly also by light exposure and temperature.

Effect of air pollution on biological colonization

Air pollution (gases, particulate matter) can affect the surface of monuments by increasing acidity and depositing new chemical compounds (various salts such as gypsum) due to the interaction of stone components with these pollutants, inducing a change in the structure of microbial communities that adapt to their new environment [12, 23, 60, 61]. The microorganisms on the surface of the stones play an important role in their degradation, and the pollutants can intensify/accelerate these effects [23, 60, 62, 63].

Rainfall analysis conducted in November 2015 and April 2016 show a high proportion of chloride in November 2015, which can be attributed to the cleaning of the tombs with bleach water. In April 2016, the proportions of ammonium, nitrate, and sulfate accounted for more than the half of the ions studied (Fig. 2). These compounds may be related to air pollution such as sulfur and NOx emissions. These pollutants can be used as nutrients by certain microorganisms, affecting their metabolism [61, 64]. NOx has been shown to favor the development to nitrogen-metabolizing bacteria. In this study, the genera *Nocardiodes*, *Friedmanniella*, *Methylobacterium-Methylorubrum*, *Sphingomonas* and *Rubellimicrobium* were found in high proportions in the sheltered position, where high nitrate concentrations were observed. Some species of the aforementioned genus have been identified as denitrifying bacteria capable of reducing nitrate compounds to nitrite [65–70]. Furthermore, the study of [71], shows the ability of a fungal community composed of the species *Cladosporium sp*., *Penicillium sp*., *Rhodotorula sp*. and *Cryptococcus sp*. to utilize sulfate compound as a nutrient. In our study, the genus *Cladosporium* is present on all samples in high proportion, this genus can promote the consumption of sulfate on limestone surface, which can explain the absence of gypsum after 5 years of exposure. Therefore, pollution influences the composition of rainwater. The actual composition tends to favor denitrifying bacteria and could provide nutrients for some fungal genera.

Alteration facies

Visually, after 5 years of exposure to the Parisian atmosphere in a green area, limestone samples exposed to rain are covered by mosses and microorganisms in horizontal position and by a green patina in vertical position. Samples sheltered from the rain are slightly gray and the biocolonization appears to be low. They are more susceptible to contamination from pollutant deposition [72–76]. Therefore, samples exposed to rain seem to be more affected by bioalteration processes, whereas sheltered samples are affected by physico-chemical processes.

However, the alteration of stone (dissolution, secondary phase formation, porosity change…) is difficult to quantify at this stage and no obvious sign of physical or chemical attack is evidenced. On sheltered positions (SH and SV), XRD analyses show the presence of

neocrystallization of potassium nitrate (KNO_3). The potassium and nitrate involved in the formation of KNO_3 seems to come from rainfall (Table 1), which is consistent with the salt growth requiring an alternation of wet and dry periods. On the positions exposed to rain (UH and UV), no secondary crystalline phases are visible due to the rain leaching. Microscopic analyses do not show the formation of secondary phases as secondary carbonates are difficult to observe and gypsum is not detectable at this stage. The loss of material and the evolution of the roughness cannot be precisely quantified due to the biocolonization.

The results obtained after 5 years can be linked to the main observations made on ancient tombs in the Père-Lachaise cemetery [23]. The horizontal parts (specimens) are mostly colonized by mosses, microalgae and bacteria and a kind of soil is formed at the surface. The vertical parts (steles) are covered by biofilms, lichens, algae… They erode when exposed to rain, and gypsum and soot can be found in more sheltered areas. Black crusts can be thick in the most sheltered parts. Therefore, bioalteration is predominant and relatively fast, while physico-chemical processes (erosion, pollution and black crusts) are slower.

In vegetated areas such as the Père Lachaise cemetery, field observations show that the most frequent alterations are erosion in areas exposed to rain, soiling or encrustation in sheltered areas, and biocolonization. With the reduction in SO_2 in Paris, rainfall is less acidic and black crusts are harder to form. Biocolonization will therefore be a major phenomenon in the future as temperatures and rainfall increase (Reboah et al. 2023). This will have to be taken into account in the conservation of monuments.

Conclusion

This work presents the results of 5 years of exposure of limestone samples in a vegetated area in different conditions (sheltered vs. unsheltered from rain, horizontally vs. vertically exposed). The characterization of the samples shows that the microbial communities are strongly present on limestone surfaces and especially on those exposed to rainfall. Sequencing of these communities revealed different phyla: Actinobacteriota, Bacteroidota, Cyanobacteria, Proteobacteria and Deinococcota for bacteria and Ascomycota for fungi. Moreover, some significant differences in the respective contributions were detected as a function of the condition (exposed to rain or not) and of the orientation (horizontal or vertical), revealing the role of water availability, light and temperature. At this stage, the only sign of physico-chemical processes (dissolution, secondary phase precipitation) is the formation of KNO_3 on sheltered samples. This phase can originate from the rainwater. Therefore, in the short-term the main cause of alteration is the biological colonization. Physical, chemical, and biogenic alteration facies are slower to be evidenced. However, it is expected that these processes will lead to a significant state of alteration, as this is observed on the ancient tombs of the cemetery.

Supplementary Information

The online version contains supplementary material available at https://doi.org/10.1186/s40494-024-01388-x.

Supplementary Material 1.

Acknowledgements
The authors would like to thank the director B. GALLOT and the conservator G. GROUD of the Père-Lachaise cemetery to give use the authorization to expose limestone specimens during five years. They also acknowledge the Agence Nationale de la Recherche (Project-ANR-19-CE22-000 MIAM) and OSU-Efluve for the financial supports. The authors thank the Prammics platform for ion chromatography analyses. The authors acknowledge the INRA MIGALE bioinformatics facility (MIGALE, INRA, 2018. Migale bioinformatics Facility, doi: 1015454/1.5572390655343293E12) for providing help and support. They also acknowledge the reviewers for their helpful comments.

Author contributions
P.R. realized and interpreted all biological experiments and was the principal writer of this manuscript A.V.C. initiated the project, interpreted rainfall analyses and is a major contributor in writing this manuscript S.A.A. have substantively revised it V.A. helped to set up samples in Père Lachaise cemetery O.L. analyzed the rainfall and soluble ions by ionic chromatography S.N. realized the crystalline phases analyses A.C. have substantively revised it M.S. initiated the project and the exposure monitoring C.B.B.B. initiated the project and is one of the major contributor in writing this manuscript All authors read and approved the final manuscript.

Funding
This study was financially supported by Agence Nationale de la recherche MIAM Project-ANR-19-CE22-0006).

Availability of data and materials
No datasets were generated or analysed during the current study.

Declarations

Competing interests
The authors declare no competing interests.

Received: 3 April 2024 Accepted: 22 July 2024
Published online: 01 August 2024

References

1. Blanc A, Gely JP, Vire M. Le calcaire lutetien, ses carrieres, son utilisation dans les monuments. In: Le lutétien, la pierre de Paris. 2000. p. 38-46.
2. Mizutani E, Ogura D, Ishizaki T, Abuku M, Sasaki J. Influence of the infiltrated rainwater on the degradation of the inner wall in Hagia Sophia. Istanbul Energy Procedia. 2015;78:1353–8.
3. Sand W. Microbial mechanisms of deterioration of inorganic substrates—a general mechanistic overview. Int Biodeterior Biodegrad. 1997;40(2–4):183–90.
4. Camuffo D. Deterioration processes of historical monuments. Stud Environ Sci. 1986;30:189–221.

5. Charola AE, Pühringer J, Steiger M. Gypsum: a review of its role in the deterioration of building materials. Environ Geol. 2007;52(2):207–20.
6. Camuffo D. Weathering of Building Materials. In: Brimblecombe P, éditeur. Urban pollution and change to Material and Building Surfaces. 2016. p. 19-59.
7. Gaylarde PM, Gaylarde CC. Algae and cyanobacteria on painted buildings in Latin America. Int Biodeterior Biodegrad. 2000;46(2):93–7.
8. González-Gómez WS, Quintana P, Gómez-Cornelio S, García-Solis C, Sierra-Fernandez A, Ortega-Morales O, et al. Calcium oxalates in biofilms on limestone walls of Maya buildings in Chichén Itzá. Mexico Environ Earth Sci. 2018;77(6):1–12.
9. Balland-Bolou-Bi C, Saheb M, Alphonse V, Livet A, Reboah P, Abbad-Andaloussi S, et al. Effect of cultivable bacteria and fungi on the limestone weathering used in historical buildings. Diversity. 2023;15(5):587.
10. Altieri A, Ricci S. Calcium uptake in mosses and its role in stone biodeterioration. Int Biodeterior Biodegrad. 1997;40(2–4):201–4.
11. Jang K, Viles H. Moisture interactions between mosses and their underlying stone substrates. Stud Conserv. 2022;67(8):532–44.
12. Scheerer S, Ortega-Morales O, Gaylarde C. Chapter 5 microbial deterioration of stone monuments-an updated overview, 1 éd. Adv Appl Microbiol. 2009;66:97–139.
13. Warscheid T, Braams J. Biodeterioration of stone: a review. Int Biodeterior Biodegrad. 2000;46(4):343–68.
14. Sterflinger K, Piñar G. Microbial deterioration of cultural heritage and works of art—tilting at windmills? Appl Microbiol Biotechnol. 2013;97(22):9637–46.
15. Pinheiro AC, Mesquita N, Trovão J, Soares F, Tiago I, Coelho C, et al. Limestone biodeterioration: a review on the Portuguese cultural heritage scenario. J Cult Herit. 2019;36:275–85.
16. De Leo F, Marchetta A, Urzì C. Black fungi on stone-built heritage: current knowledge and future outlook. Appl Sci Switz. 2022;12(8):3969.
17. Fitzner B, Heinrichs K. Damage diagnosis at stone monuments—weathering forms, damage categories and damage indices. Acta Univ Carol Geol. 2001;45(1):12–3.
18. Fehér K, Török Á. Detecting short-term weathering of stone monuments by 3D laser scanning: lithology, wall orientation, material loss. J Cult Herit. 2022;58:245–55.
19. Eyssautier-Chuine S, Vaillant-Gaveau N, Charpentier E, Reffuveille F. Comparison of biofilm development on three building and restoration stones used in French monuments. Int Biodeterior Biodegrad. 2021;165(August):1–10.
20. Eyssautier-Chuine S, Mouhoubi K, Reffuveille F, Bodnar JL. Thermographic imaging for early detection of biocolonization on buildings. Build Res Inf. 2020;48(8):856–65.
21. Miller AZ, Laiz L, Gonzalez JM, Dionísio A, Macedo MF, Saiz-Jimenez C. Reproducing stone monument photosynthetic-based colonization under laboratory conditions. Sci Total Environ. 2008;405(1–3):278–85.
22. Miller AZ, Dionísio A, Laiz L, MacEdo MF, Saiz-Jimenez C. The influence of inherent properties of building limestones on their bioreceptivity to phototrophic microorganisms. Ann Microbiol. 2009;59(4):705–13.
23. Balland-Bolou-Bi C, Saheb M, Bousserrhine N, Abbad-Andaloussi S, Alphonse V, Nowak S, et al. Effect of microorganism activities in a polluted area on the alteration of limestone used in historical buildings. In: ICDCS 2016 science and art : a future for stone_vol1. 2016. p. 25-32.
24. Rozenbaum O, Barbanson L, Muller F, Bruand A. Significance of a combined approach for replacement stones in the heritage buildings' conservation frame. Comptes Rendus Geosci. 2008;340(6):345–55.
25. Saheb M, Chabas A, Mertz JD, Colas E, Rozenbaum O, Sizun JP, et al. Weathering of limestone after several decades in an urban environment. Corros Sci. 2016;111:742–52.
26. Keene WC, Pszenny AAP, Galloway JN, Hawley ME. Sea-salt corrections and interpretation of constituent ratios in marine precipitation. J Geophys Res Atmos. 1986;91(D6):6647–58.
27. Rudnick RL, Gao S. Composition ofthe Continental Crust. In: Holland HD, Turekian KK, éditeurs. Treatise on geochemistry. 2014. p. 1-64.
28. Reboah P, Bolou-Bi CB, Nowak S, Verney-Carron A. Influence of climatic factors on cyanobacteria and green algae development on building surface. PLoS ONE. 2023;18:1–19.
29. Sutton S. The most probable number method and its uses in enumeration, qualification, and validation. J Valid Technol. 2010;8-41.
30. Jarvis B, Wilrich C, Wilrich PT. Reconsideration of the derivation of Most Probable Numbers, their standard deviations, confidence bounds and rarity values. J Appl Microbiol. 2010;109(5):1660–7.
31. Steinfeld JI, Pandis SN. Atmospheric chemistry and physics: from air pollution to climate change. Environ Sci Policy Sustain Dev. 1998;40(7):26–26.
32. Whelpdale DM, Summers PW, Sanhueza E. A global overview of atmospheric acid deposition fluxes. Environ Monit Assess. 1997;48(3):217–47.
33. Keresztesi Á, Birsan MV, Nita IA, Bodor Z, Szép R. Assessing the neutralisation, wet deposition and source contributions of the precipitation chemistry over Europe during 2000–2017. Environ Sci Eur. 2019;31(1):1–15.
34. Niu Y, Li X, Huang Z, Zhu C. Chemical characteristics and possible causes of acid rain at a regional atmospheric background site in eastern China. Air Qual Atmos Health. 2017;10(8):971–80.
35. Beysens D, Mongruel A, Acker K. Urban dew and rain in Paris, France: Occurrence and physico-chemical characteristics. Atmos Res. 2017;189:152–61.
36. Caroll D. Rainwater as a chemical agent of geologic processes—a review|resolution copper project and land exchange environmental impact statement. 1962.
37. Salve PR, Maurya A, Wate SR, Devotta S. Chemical composition of major ions in rainwater. Bull Environ Contam Toxicol. 2008;80(3):242–6.
38. Decina SM, Templer PH, Hutyra LR. Atmospheric inputs of nitrogen, carbon, and phosphorus across an urban area: unaccounted fluxes and canopy influences. Earths Future. 2018;6(2):134–48.
39. Thornton JA, Kercher JP, Riedel TP, Wagner NL, Cozic J, Holloway JS, et al. A large atomic chlorine source inferred from mid-continental reactive nitrogen chemistry. Nat. 2010;464(7286):271–4.
40. Kumar R, Rani A, Singh SP, Maharaj K, Srivastava SS. A long term study on chemical composition of rainwater at Dayalbagh, a suburban site of semiarid region. J Atmospheric Chem. 2002;41(3):265–79.
41. Sun X, Wang Y, Li H, Yang X, Sun L, Wang X, et al. Organic acids in cloud water and rainwater at a mountain site in acid rain areas of South China. Environ Sci Pollut Res. 2016. https://doi.org/10.1007/s11356-016-6038-1.
42. Chebbi A, Carlier P. Carboxylic acids in the troposphere, occurrence, sources, and sinks: a review. Atmos Environ. 1996;30(24):4233–49.
43. Macedo MF, Miller AZ, Dionísio A, Saiz-Jimenez C. Biodiversity of cyanobacteria and green algae on monuments in the Mediterranean Basin: an overview. Microbiology. 2009;155(11):3476–90.
44. Barberousse H, Lombardo RJ, Tell G, Couté A. Factors involved in the colonisation of building façades by algae and cyanobacteria in France. Biofouling. 2006;22(2):69–77.
45. Gambino M, Lepri G, Štovícek A, Ghazayarn L, Villa F, Gillor O, et al. The tombstones at the Monumental Cemetery of Milano select for a specialized microbial community. Int Biodeterior Biodegrad. 2021;164(January):105298.
46. Coelho C, Mesquita N, Costa I, Soares F, Trovão J, Freitas H, et al. Bacterial and archaeal structural diversity in several biodeterioration patterns on the limestone walls of the old cathedral of coimbra. Microorganisms. 2021;9(4):709.
47. Mihajlovski A, Gabarre A, Seyer D, Bousta F, Di Martino P. Bacterial diversity on rock surface of the ruined part of a French historic monument: the Chaalis abbey. Int Biodeterior Biodegrad. 2017;120:161–9.
48. Ding Y, Salvador CSC, Caldeira AT, Angelini E, Schiavon N. Biodegradation and microbial contamination of limestone surfaces: an experimental study from Batalha monastery. Portugal Corros Mater Degrad. 2021;2(1):31–45.
49. McNamara CJ, Perry TD IV, Bearce KA, Hernandez-Duque G, Mitchell R. Epilithic and endolithic bacterial communities in limestone from a Maya archaeological site. Microb Ecol. 2006;51(1):51–64.
50. Silva NC, Madureira AR, Pintado M, Moreira PR. Biocontamination and diversity of epilithic bacteria and fungi colonising outdoor stone and mortar sculptures. Appl Microbiol Biotechnol. 2022;106(9–10):3811–28.
51. Li Q, Zhang B, He Z, Yang X. Distribution and diversity of bacteria and fungi colonization in stone monuments analyzed by high-throughput sequencing. PLoS ONE. 2016;11(9):1–17.
52. Wang Y, Liu X. Sulfur-oxidizing bacteria involved in the blackening of basalt sculptures of the Leizhou Stone Dog. Int Biodeterior Biodegrad. 2021;159(February):105207.
53. Green PN. Methylobacterium. Bergeys Man Syst Archaea Bact. 2015;1-8.
54. Balland-Bolou-Bi C, Bolou-Bi EB, Alphonse V, Giusti-Miller S, Jusselme MD, Livet A, et al. Impact of microbial activity on the

mobility of metallic elements (Fe, Al and Hg) in tropical soils. Geoderma. 2018;2019(334):146–54.
55. Rosado T, Dias L, Lança M, Nogueira C, Santos R, Martins MR, et al. Assessment of microbiota present on a Portuguese historical stone convent using high-throughput sequencing approaches. MicrobiologyOpen. 2020;9(6):1067–84.
56. Bernardet JF, Bowman JP. The prokaryotes, the genus flavobacterium. The prokaryotes: proteobacteria: delta and epsilon subclasses. Deeply Rooting Bacteria. 2006. 481–531. https://doi.org/10.1007/0-387-30747-8_17
57. Pitzurra L, Moroni B, Nocentini A, Sbaraglia G, Poli G, Bistoni F. Microbial growth and air pollution in carbonate rock weathering. Int Biodeterior Biodegrad. 2003;52(2):63–8.
58. Paiva DS, Fernandes L, Trovão J, Mesquita N, Tiago I, Portugal A. Uncovering the fungal diversity colonizing limestone walls of a forgotten monument in the central region of portugal by high-throughput sequencing and culture-based methods. Appl Sci Switz. 2022;12(20):10650.
59. Thüs H, Muggia L, Pérez-Ortega S, Favero-Longo SE, Joneson S, O'Brien H, et al. Revisiting photobiont diversity in the lichen family verrucariaceae (ascomycota). Eur J Phycol. 2011;46(4):399–415.
60. Schröer L, De Kock T, Cnudde V, Boon N. Differential colonization of microbial communities inhabiting Lede stone in the urban and rural environment. Sci Total Environ. 2020;733:139339.
61. Villa F, Vasanthakumar A, Mitchell R, Cappitelli F. RNA-based molecular survey of biodiversity of limestone tombstone microbiota in response to atmospheric sulphur pollution. Lett Appl Microbiol. 2015;60(1):92–102.
62. Ortega-Morales O, Montero-Muñoz JL, Baptista Neto JA, Beech IB, Sunner J, Gaylarde C. Deterioration and microbial colonization of cultural heritage stone buildings in polluted and unpolluted tropical and subtropical climates: A meta-analysis. Int Biodeterior Biodegrad. 2019;143(July):104734.
63. Gaylarde C, Baptista-Neto JA, Ogawa A, Kowalski M, Celikkol-Aydin S, Beech I. Epilithic and endolithic microorganisms and deterioration on stone church facades subject to urban pollution in a sub-tropical climate. Biofouling. 2017;33(2):113–27.
64. Sazanova KV, Zelenskaya MS, Vlasov AD, Bobir SY, Yakkonen KL, Vlasov DY. Microorganisms in superficial deposits on the stone monuments in saint petersburg. Microorganisms. 2022;10(2):316.
65. Cua LS, Stein LY. Characterization of denitrifying activity by the alphaproteobacterium, *Sphingomonas wittichii* RW1. Front Microbiol. 2014;5:1–7.
66. Yun L, Yu Z, Li Y, Luo P, Jiang X, Tian Y, et al. Ammonia nitrogen and nitrite removal by a heterotrophic Sphingomonas sp strain LPN080 and its potential application in aquaculture. Aquaculture. 2018;2019(500):477–84.
67. Alessa O, Ogura Y, Fujitani Y, Takami H, Hayashi T, Sahin N, et al. Comprehensive comparative genomics and phenotyping of methylobacterium species. Front Microbiol. 2021;12(October):1–21.
68. Iwai K, Aisaka K, Suzuki M. *Friedmanniella luteola* sp. nov., *Friedmanniella lucida* sp. nov., *Friedmanniella okinawensis* sp. nov. and *Friedmaniella sagamiharensis* sp. nov., isolated from spiders. Int J Syst Evol Microbiol. 2010;60(1):113–20.
69. Cui Y, Woo SG, Lee J, Sinha S, Kang MS, Jin L, et al. *Nocardioides daeguensis* sp. nov., a nitratereducing bacterium isolated from activated sludge of an industrial wastewater treatment plant. Int J Syst Evol Microbiol. 2013;63(PART10):3727–32.
70. Xing W, Li J, Li D, Hu J, Deng S, Cui Y, et al. Stable-isotope probing reveals the activity and function of autotrophic and heterotrophic denitrifiers in nitrate removal from organic-limited wastewater. Environ Sci Technol. 2018. https://doi.org/10.1021/acs.est.8b01993.
71. Moroni B, Pitzurra L. Biodegradation of atmospheric pollutants by fungi: a crucial point in the corrosion of carbonate building stone. Int Biodeterior Biodegrad. 2008;62(4):391–6.
72. Beloin NJ, Haynie FH. Soiling of building materials. J Air Pollut Control Assoc. 1975;25(4):399–403.
73. Pio CA, Lopes DA. Chlorine loss from marine aerosol in a coastal atmosphere. J Geophys Res Atmospheres. 1998;103(D19):25263–72.
74. Grossi CM, Esbert RM, Díaz-Pache F, Alonso FJ. Soiling of building stones in urban environments. Build Environ. 2003;38(1):147–59.
75. Watt J, Hamilton R. The soiling of buildings by air pollution. In: The effects of air pollution on the built environment. 2003. p. 289-334. https://doi.org/10.1142/9781848161283_0010
76. Creighton PJ, Lioy PJ, Haynie FH, Lemmons TJ, Miller JL, Gerhart J. Soiling by atmospheric aerosols in an urban industrial area. J Air Waste Manag Assoc. 1990;40(9):1285–9.

Publisher's Note